Base-paired structure in the 5' untranslated region is required for the efficient amplification of negative-strand RNA3 in the bromovirus melandrium yellow fleck virus.

AUTHOR(S):

Narabayashi, Taiki; Kaido, Masanori; Okuno, Tetsuro; Mise, Kazuyuki

CITATION:

Narabayashi, Taiki ...[et al]. Base-paired structure in the 5' untranslated region is required for the efficient amplification of negative-strand RNA3 in the bromovirus melandrium yellow fleck virus.. Virus research 2014, 188: 162-169

ISSUE DATE:

2014-08-08

URL:

http://hdl.handle.net/2433/189276

Base-paired structure in the 5′ untranslated region is required for the efficient amplification of negative-strand RNA3 in the bromovirus melandrium yellow fleck virus

Taiki Narabayashi, Masanori Kaido, Tetsuro Okuno, Kazuyuki Mise *

Laboratory of Plant Pathology, Graduate School of Agriculture, Kyoto University, Kyoto 606-8502, Japan

* Corresponding author at: Laboratory of Plant Pathology, Graduate School of Agriculture, Kyoto University, Kitashirakawa, Sakyo-ku, Kyoto 606-8502, Japan. Tel: +81-75-753-6132; Fax: +81 75 753 6131.

E-mail address: kmise@kais.kyoto-u.ac.jp (K. Mise).

ABSTRACT

Melandrium yellow fleck virus belongs to the genus *Bromovirus*, which is a group of tripartite plant RNA viruses. This virus has an approximately 200-nucleotide direct repeat sequence in the 5′ untranslated region (UTR) of RNA3 that encodes the 3a movement protein. In the present study, protoplast assays suggested that the duplicated region contains amplification-enhancing elements. Deletion analyses of the 5′ UTR of RNA3 showed that mutations in the short base-paired region, which is located dozens of bases upstream of the initiation codon of the 3a gene, greatly reduced the accumulation of RNA3. Disruption and restoration of the base-paired structure caused the accumulation of RNA3 to be decreased and restored, respectively. In vitro translation/replication assays demonstrated that the base-paired structure is important for the efficient amplification of negative-stand RNA3. A similar base-paired structure in RNA3 of another bromovirus, brome mosaic virus (BMV), also facilitated the efficient amplification of BMV RNA3, but only in combination with melandrium yellow fleck virus (MYFV) replicase and not with BMV replicase, thereby suggesting specific interactions between base-paired structures and MYFV replicase.

Keywords: 5′ untranslated region; *Bromovirus*; positive-strand RNA virus; protoplast; RNA replication; RNA structure

1. Introduction

The genomic RNAs of all positive-strand RNA viruses have multifunctional roles. They act as mRNAs to translate viral proteins and also as the templates for negative-strand RNA synthesis. Thus, it is important to regulate these processes, and several RNA elements have been identified that are required for these processes (Dreher, 1999; Liu et al., 2009; Noueiry and Ahlquist, 2003; Ogram and Flanegan, 2011; Pathak et al., 2011). Negative-strand RNA synthesis is initiated near the 3′ terminus, but the RNA elements required for negative-strand RNA synthesis are located in the other regions of viral RNAs such as the 5′ untranslated region (UTR), as well as in the 3′ UTR. The functions of these RNA elements have been investigated, and they are known to be regulated by interactions between viral RNA elements, or between viral RNA elements and proteins, including viral and host factors (Filomatori et al., 2006; Herold and Andino, 2001; Noueiry and Ahlquist, 2003; Pathak et al., 2011).

Brome mosaic virus is the type species of the genus *Bromovirus*, which is a group of icosahedral plant RNA viruses in the family *Bromoviridae*. The genome comprises three genomic RNAs, which are referred to as RNA1, RNA2, and RNA3 in order of their genome sizes. RNA1 and RNA2 are monocistronic RNAs that encode the 1a and 2a proteins, respectively, and both are required for genomic and subgenomic RNA4 synthesis (Kroner et al., 1989; 1990). RNA3 is a dicistronic RNA that encodes the 3a protein required for bromovirus movement (Mise et al., 1993) and the coat protein, which is translated from the RNA4 that is transcribed from the negative-strand RNA3 (Miller et al., 1985).

The *cis*-acting RNA elements required for the negative-strand synthesis of brome mosaic virus (BMV) genomic RNAs are well characterized. In the 3′ UTR, the stem loop C within the tRNA-like structure acts as the promoter for negative-strand synthesis (Kim et al., 2000). The box B motif in the intercistronic region of RNA3 is recognized by the 1a protein, and

RNA3 is recruited to endoplasmic reticulum membrane invaginations where BMV replication occurs (Schwartz et al., 2002; Sullivan and Ahlquist, 1999). The requirement for both the intercistronic region and the 3′ UTR of RNA3 for the formation of the replicase complex was demonstrated in a yeast system (Quadt et al., 1995), which fully supports BMV replication and transcription, as found in plant cells (Janda and Ahlquist, 1993). The 5′ UTR of RNA2 also contains the box B motif, and it has been reported to be involved in translational repression and RNA recruitment, which are key steps during negative-strand RNA synthesis (Chen et al., 2001; Yi et al., 2007). However, although the 5′ UTR of RNA3 was also shown to be important for negative-strand RNA3 accumulation (Choi et al., 2004), the detailed roles of the 5′ UTR of RNA3 in negative-strand synthesis have remained unclear.

Previously, we constructed infectious cDNA clones for the bromovirus melandrium yellow fleck virus (MYFV) and determined their nucleotide sequences, which showed that the genomic RNA3 of MYFV has unique characteristics compared with those of other bromoviruses (Narabayashi et al., 2009). Unlike BMV RNA3 having a poly(A) tract in the intercistronic region between the 3a and coat protein genes, MYFV RNA3 lacks the poly(A) tract, and it contains a duplicated sequence of about 200 bases with a short ORF around the border of the duplicated regions in the 5′ UTR. During cDNA cloning procedures, we also found that 10% of the cDNA clones lacked the duplication in the 5′ UTR of RNA3. These minor clones had nucleotide sequences identical to those of the other major clones except for the duplication. Co-infection experiments using RNA3 clones with or without the duplicated sequence (3W and 3S, respectively, in Fig. 1A) demonstrated that the duplication contributed to the competitive fitness of the virus in *Nicotiana benthamiana* plants (Narabayashi et al., 2009). However, the functional role of this duplication in MYFV life cycles has not been determined. In this study, we used both *N. benthamiana* protoplasts in vivo and an evacuolated BY-2 protoplast lysate (BYL) in vitro (Komoda et al., 2004) and identified a

novel RNA element within the duplicated region in the 5′ UTR of MYFV RNA3, which is required for the efficient amplification of MYFV RNA3, probably by enhancing negative-strand amplification via specific interactions with its cognate replicase.

2. Materials and methods

2.1. Plasmid construction

The pMY3TP4 (3S) contains the same cDNA insert found in pMY3TP3 (3W), except it lacks the duplicated region (Narabayashi et al., 2009). Before creating a series of plasmids that encoded the C-terminal hemagglutinin (HA)-tagged 3a protein, we inserted three nucleotides (GGC) that encoded a glycine spacer sequence and a HA-coding nucleotide sequence (TACCCATACGATGTTCCAGATTACGCT) immediately upstream of the stop codon of the 3a gene in pMY3TP4 (3S), thereby generating pMY3TP4-HA.

All of the primers used in this study are shown in Supplementary Table S1. The plasmids with mutations in the 5′ UTR of MYFV RNA3 were generated by PCR-mediated site-directed mutagenesis of pMY3TP4-HA, which is a method referred to as “recombinant PCR” (Higuchi, 1990). The two pairs of primers used for primary PCR to amplify two DNA fragments were M4 plus dn_R and dn_F plus MY3.13R-2 (n = 55–153, 104–202, 154–226, 154–252, 55–64, 65–81, 82–103, 203–217, and 218–229). The two resultant DNA fragments were recombined by secondary PCR using M4 plus MY3.13R-2. The amplified DNA fragments were purified, digested with *Hin*dIII and *Acc*I, and ligated into *Hin*dIII and *Acc*I-cut pMY3TP4-HA to generate pMY3TP4-HA-dn (n = 55–153, 104–202, 154–226, 154–252, 55–64, 65–81, 82–103, 203–217, and 218–229). The following seven plasmids were constructed in a similar manner using two or three pairs of appropriate primers for primary PCR. pMY3TP4-HA-rx (x = 1–1,

1–2, 2–1, and 2–2) was constructed using two pairs of primers: M4 plus rx_R and rx_F plus MY3.13R-2 (x = 1–1, 1–2, 2–1, and 2–2). pMY3TP4-HA-dMB-1 was constructed using three pairs of primers: M4 plus dMB-1_4, dMB-1_1 plus dMB-1_3, and dMB-1_2 plus MY3.13R-2. pMY3TP4-HA-dMB-2 and pMY3TP4-HA-dMB-3 were constructed using two pairs of primers: M4 plus dMB-2_2 and dMB-2_1 plus MY3.13R-2, or M4 plus dMB3_R and dMB3_F plus MY3.13R-2, respectively.

To construct pBYL2MY1a and pBYLMY2a, cDNA fragments containing the 1a and 2a genes were PCR-amplified from pMY1TP1 and pMY2TP2 (Narabayashi et al., 2009) using two pairs of primers: pBYL-MY1a_F plus pBYL-MY1a_R and pBYL-MY2a_F plus pBYL-MY2a_R (Supplementary Table S1), respectively. The amplified fragments were digested with *Asc*I and ligated into *Asc*I-cut pBYL2 (Mine et al., 2010) in the correct orientation.

BMV derivatives were generated by PCR-mediated site-directed mutagenesis of pB3TP8 (Janda et al., 1987) using the primer pairs Bd1_F plus Bd1_R and Bd2_F plus Bd2_R (Supplementary Table S1). The amplified fragments were digested with *Cla*I and *Sph*I, and ligated into *Cla*I and *Sph*I-cut pB3TP8 to generate pB3TP8-Bd1 and pB3TP8-Bd2, respectively.

2.2. In vitro transcription and protoplast experiments

Transcripts of bromoviral RNAs were synthesized using T7 RNA polymerase (Takara, Otsu, Japan) with the appropriate cap structure analog (m^7GpppG; New England Biolabs, Beverly, MA, USA), as described previously (Kroner and Ahlquist, 1992; Narabayashi et al., 2009). mRNAs encoding MYFV 1a and 2a proteins were synthesized from *Not*I-linearized pBYLMY1a and pBYLMY2a, respectively. All of the transcripts were purified using

Sephadex G-50 (GE Healthcare Bio-Sciences Corp., Piscataway. NJ, USA) gel chromatography.

N. benthamiana protoplast assays were performed as described previously (Narabayashi et al., 2009). Typically, 2–3 × 10^5 protoplasts were inoculated with 3.0 μg of transcripts (1 μg each of RNA1, RNA2, and RNA3) and incubated for 20 h.

2.3. Northern blot analysis

Northern blot analysis of the total RNA was performed as described previously (Narabayashi et al., 2009). To construct pMY3ES504 for detecting the negative strand of MYFV RNA3, the 0.4–kb *Sac*I/*Eco*RV fragments of pMY3TP3 were cloned into pBluescript II (SK-) (Stratagene, La Jolla, CA). The negative-strand MYFV RNA3 was detected using digoxigenin (DIG)-labeled T7 transcripts from *Eco*RV-linearized pMY3ES504. The positive-strand BMV RNAs were detected using DIG-labeled riboprobes, which recognized the 3′ terminal region of all BMV RNAs (Kaido et al., 1995).

2.4. BYL experiments

The preparation of BYL and the in vitro translation/replication reaction were performed as described previously (Iwakawa et al., 2007; Komoda et al., 2004). The mRNAs encoding 1a and 2a proteins, which were transcribed from pBYL2-MY1a and pBYL-MY2a, respectively, were incubated in BYL at 25 °C for 2 h. Aliquots (24 μl) of the reaction mixture were incubated further with bromovirus RNA3 and its derivatives at 25 °C for 2 h. The total RNAs were then extracted and used for the Northern blot analysis.

For RNA stability assay, 0.5 μg of capped transcripts were incubated at 25 °C in 40 μl of

BYL reaction mixture. At 0, 0.5, 1 and 2 h after incubation, aliquots (10 µl) were used for RNA extraction, and subjected to Northern blot analysis.

3. Results

3.1. The 3W levels were higher than the 3S levels in a competition assay using N. benthamiana protoplasts

We assumed that the differences in competitive fitness between 3W and 3S in whole *N. benthamiana* plants (Narabayashi et al., 2009) might reflect the replication efficiency at the single-cell levels. To verify this assumption, we inoculated *N. benthamiana* protoplasts with an equimolar mixture of 3W and 3S, and RNAs 1 and 2 of MYFV. The Northern blot analysis showed that the levels of RNA3 were similar after individual infection with 3W or 3S, whereas 3W accumulated to 30% higher than 3S following coinfection (Figs. 1B and 1C). This suggests that there is competition for replication between 3W and 3S, and that the competitive fitness is determined at least partly during the replication step. Given that both of the 5′ and 3′ terminal regions, as well as intercistronic regions, are required for the efficient amplification of BMV RNA3s (French and Ahlquist, 1987), this duplicated region in the internal site of the 5′ UTR of MYFV RNA3 might contain previously undefined element(s) that enhance the efficient amplification of bromoviral RNA3.

3.2. Regions in the 5′ UTR required for efficient amplification of RNA3

To identify the putative *cis*-acting replication elements in the duplicated region (nt 55–

252), we constructed RNA3 derivatives that contained a series of 100-base deletions in the 5′ UTR and the 5′ proximal sequences of the 3a-ORF (d55–153, d104–202, and d154–252; Fig. 2A). To exclude the possibility that the effects of the deletion of one element in the duplicated region (light gray region in Fig. 1A) on RNA3 accumulation may have been masked or attenuated by another element because of the duplication in 3W, we introduced deletions into the 5′ UTR of 3S (dark gray region in Fig. 1A) but not into that of 3W. The resultant RNA3 derivatives, and RNA1 and RNA2, were inoculated into *N. benthamiana* protoplasts, and the accumulation of MYFV RNAs was analyzed by Northern blotting. The d55–153 and d154–252 mutations, but not the d104–202 mutation, reduced the accumulation of RNA3 and RNA4 in protoplasts (Fig. 2B). These results suggest that the two regions, i.e., one from nt 55–103 and the other from nt 203–252, contain nucleotide sequences and/or structures that play important roles in the accumulation of RNA3 and RNA4.

The d154–252 mutant lacked a partial 5′ coding sequence from the 3a gene, so we examined whether this short coding region had any functions during RNA3 accumulation. A d154–226 mutant was constructed with a deletion in the same region as d154–252 apart from the 5′ coding region of the 3a gene, which was tested in *N. benthaminana* protoplasts. The accumulation of RNA3 and RNA4 from d154–226 was comparable to that of RNA3 and RNA4 from d154–252 (Fig. 2B), thereby suggesting that deletions in the 5′ UTR of MYFV RNA3 but not the 3a-coding region reduced the accumulation of RNA3 and RNA4 dramatically. Subsequently, we focused on the functions of the 5′ UTR of MYFV RNA3 during RNA3 accumulation.

To characterize further the RNA elements involved in RNA3 accumulation, we predicted the secondary RNA structures in the 5′ UTR of RNA3 using M-fold version 3.2 (Zuker, 2003), which showed that the two regions (one from nt 55–103 and the other from nt 203–252) formed a long base-paired structure with each other (Fig. 3A). To delimit the regions that

could affect the accumulation of RNA3, we constructed five mutants with deletions covering the two regions in the 5′ UTR of RNA3 (d55–64, d65–81, d82–103, d203–217, and d218–229; Fig. 3B), and we examined their accumulation in *N. benthamiana* protoplasts when they were inoculated together with MYFV RNA1 and RNA2 transcripts. Three deletions (nt 55–64, nt 65–81, and nt 218–229) did not affect the accumulation of RNA3 or RNA4, whereas two deletions (nt 82–103 and nt 203–217) reduced the levels of RNA3 and RNA4 greatly (Fig. 3C). These two sequences were predicted to form a base-paired structure with each other, which was divided into two stems by an internal loop, thereby suggesting that either or both stems were important for the accumulation of RNA3 and RNA4.

To identify the functional domain and to determine the importance of the base-paired structure for the accumulation of RNA3, we introduced nucleotide substitutions into either or both sides of the two stems in this region, which disrupted or restored the base-pairing of the stems, respectively (Fig. 4A). Disruption of the upper stem structure on either side of this region by nucleotide substitutions (r1–1, r1–2) severely decreased the accumulation of RNA3 and RNA4, whereas the restoration of the stem (r1–3) restored the RNA3 and RNA4 levels to that of 3S in *N. benthamiana* protoplasts (Figs. 4B and 4C). Furthermore, these mutations also affected the accumulation of negative-strand RNA3 in parallel with that of positive-strand RNA3 (Figs. 4B and 4C). In contrast to the upper stem, the mutations in the lower stem (r2–1, r2–2, r2–3) did not affect the accumulation of positive- or negative-strand RNA3 (Fig. 4B). Overall, these results suggest that the upper stem structure plays a crucial role in the in vivo accumulation of positive- and negative-strand RNA3.

3.3. The base-paired structure is involved in the efficient amplification of negative-strand RNA3

The mutations in the base-paired structure reduced the in vivo accumulation of negative-strand RNA3 (Fig. 4), but it was still unclear whether this reduction was caused by decreases in negative- and/or positive-strand RNA3 synthesis. To determine whether this base-paired structure has a role in the amplification of negative-strand RNA3, we performed an in vitro translation/replication BYL assay (Komoda et al., 2004). RNA3 derivatives were incubated in BYL that expressed the 1a and 2a proteins of MYFV, and the positive- and negative-strand RNA accumulation levels were examined. Similar to the in vivo results (Fig. 4), the accumulation of negative-strand RNA3 in BYL was again reduced significantly by the disruption mutations (r1–1, r1–2) and recovered by the restoration mutation (r1–3) (Fig. 5). However, the levels of positive-strand RNA3 in BYL were not changed significantly by either the disruption (r1–1, r1–2) or restoration (r1–3) of the structure in either the presence or absence of the 1a and 2a proteins of MYFV (Fig. 5A, Supplementary Figure S2, data not shown). Together, these results mainly reflected the stability of the input transcripts rather than the levels of newly synthesized positive-strand RNA3, as discussed below. These in vitro results suggest that the reduction in negative-strand accumulation in protoplasts was attributable at least partly to a reduction in the efficient amplification of negative-strand RNA3 but not necessarily to the indirect effect of the inefficient amplification of positive-strand RNA3. These results also suggest that this base-paired region (nt 89–95 and nt 203–209) in the 5′ UTR of RNA3 is involved in the efficient amplification of negative-strand RNA3, thereby affecting the accumulation of both negative- and positive-strand RNA3s and subgenomic RNA4 in protoplasts (Fig. 4B).

3.4. Comparison between MYFV and other bromoviruses

Next, we investigated whether the base-paired structure of the 5′ UTR of RNA3 was also

seen in other bromoviruses. In the 5′ UTRs of bromoviruses, base-paired structures that comprised 7–8 base pairs containing the initiation codon (AUG) of 3a-ORF were predicted using the M-fold program (Fig. 6A). The base-paired structure of MYFV did not contain the AUG sequence, but the four consecutive base pairs (5′-UCGG-3′)/(5′-CCGA-3′) were conserved among MYFV, BMV, and cowpea chlorotic mottle virus (CCMV) (Fig. 6A). In addition, the results shown in Fig. 4 demonstrate the importance of the structure rather than the sequence for the efficient amplification of MYFV RNA3. Thus, we hypothesize that these base-paired structures may have functions during the efficient amplification of bromoviral RNA3.

To test whether a similar base-paired structure in RNA3 of another bromovirus, BMV, functions during the amplification of MYFV RNA3, we introduced mutations into the 5′ UTR of MYFV RNA3. The d-MB1 mutation deleted most of the base-paired structure, except for three G-C pairs (nt 65–92 and nt 206–229 deletions). The d-MB2 mutation was a four-base insertion into d-MB1, which formed a base-paired structure similar to that in BMV. The d-MB3 mutation replaced the base-paired region of MYFV with the corresponding region of the BMV sequence (Fig. 6B). These mutants were tested to determine their accumulation levels in *N. benthamiana* protoplasts, which were inoculated together with MYFV RNA1 and RNA2 transcripts, as described above. Northern blot analysis showed that RNA3 accumulation was eliminated by the d-MB1 mutation, whereas it was restored by the d-MB2 and d-MB3 mutations (Fig. 6C). These results suggest that the base-paired structure of MYFV RNA3 can be replaced with the corresponding structure of BMV RNA3, thereby confirming the importance of the structure rather than the sequence.

To determine whether the base-paired structure of BMV RNA3 is involved in the efficient amplification of the parental genome, two deletion mutations were introduced into the 5′ UTR of BMV RNA3 (Bd1: nt 79–91 and Bd2: nt 53–91), which resulted in disruptions

of the base-paired structure of BMV (Fig. 6D). When these mutants were inoculated together with BMV RNA1 and RNA2 into *N. benthamiana* protoplasts, the deletions slightly reduced RNA3 accumulation and increased RNA4 accumulation (Fig. 6E). BMV RNA3 could be replicated after inoculation with MYFV RNA1 and RNA2 (Fig. 6E), so we also examined the accumulation of Bd1 and Bd2 in the presence of MYFV RNA1 and RNA2. The deletions eliminated the accumulation of RNA3 and RNA4 (Fig. 6E). Thus, the base-paired structure of BMV RNA3 was essential for the efficient amplification of RNA3 by MYFV replicase, whereas this structure was not crucial for RNA3 amplification by BMV replicase. These results suggest that the function of the base-paired structure is correlated with the properties of the MYFV replicase.

4. Discussion

In the present study, we analyzed RNA elements in the 5′ UTR of bromoviral RNA3 that enhance RNA3 amplification. The function of the RNA element required for the efficient amplification of the negative-strand RNA3 of MYFV was shown to be sequence independent but structure dependent, and it was identified as the base-paired structure in the 5′ UTR of MYFV RNA3, analogues of which were also found in other bromoviral RNA3s. Our analysis of the effects of structural elements in BMV RNA3 demonstrated that the requirement for base-paired structures for RNA3 amplification differed among distinct bromoviral replicases.

The 5′ UTR of positive-strand RNA genomes corresponds to the 3′ UTR of the negative strand, which contains a promoter for positive-strand RNA synthesis. Thus, mutations in the 5′ UTR could affect positive-strand RNA synthesis. In BMV, mutations in the 5′ UTR of RNA3, which affected the promoter activity of positive-strand RNA3 synthesis, had only modest effects on negative-strand RNA3 accumulation, despite the low accumulation of

positive-strand RNA3s (Hema and Kao, 2004). Moreover, several mutations that substantially decreased positive-strand RNA3 accumulation increased subgenomic RNA4 accumulation (Grdzelishvili et al., 2005; Hema and Kao, 2004). These viral RNA accumulation patterns were also observed in our deletion analysis of the base-paired structure of BMV RNA3 when it was inoculated with BMV RNAs 1 and 2 (Fig. 6E). Thus, if the base-paired structure of the 5′ UTR of bromoviral RNA3 functions during positive-strand synthesis but not during negative-strand synthesis, mutations in this structure should change the levels of positive-strand RNA3 relative to that of subgenomic RNA4 but would have only mild effects on negative-strand accumulation. However, disruptions of the base-paired structures of the 5′ UTR of RNA3s dramatically reduced the accumulation of negative- and positive-strand RNA3 and subgenomic RNA4 in vivo (Figs. 4, 6C, and 6E). Therefore, although we cannot exclude the possibility that the base-paired structures may play an additional role in positive-strand RNA3 synthesis by MYFV replicase, similar to that by BMV replicase, the results of the protoplast assays strongly suggest that the base-paired structure functions mainly during the efficient amplification of negative-strand RNA3.

In the in vitro BYL assays, the accumulation of positive-strand RNA3 was indistinguishable among 3S and its derivatives (Fig. 5), which did not correlate with that of negative-strand RNA3. Capped transcripts are stable in BYL, and large portions of input transcripts could be detected even after incubation for several hours (Supplementary Figure S2; Sarawaneeyaruk et al., 2009). Moreover, RNA4 accumulation was never observed (data not shown), suggesting that positive-strand RNA synthesis from negative-strand RNA3 was negligible. Therefore, most, if not all, of the positive-stranded RNA3s detected reflected input transcripts, which indicated that the low accumulation of negative-strand RNA3 in vitro was not a major consequence of the indirect effects of low positive-strand RNA3 synthesis. These in vitro results support the in vivo results obtained with protoplasts, and they also indicate that

the base-paired region in the 5′ UTR of MYFV RNA3 is involved in the efficient amplification of negative-strand RNA3. Efficient amplification of negative-strand RNA3 results from efficient synthesis and/or high stability of negative-strand RNA3. If stable double-stranded RNA but not free/naked negative-strand RNA would be generated as a result of negative strand synthesis during MYFV replication like tombusvirus replication (Kovalev et al., 2014), the base-paired structure in the 5'UTR may function in synthesizing negative strand RNA3 rather than conferring stability on the nascent negative-strand RNA3.

The 5′ UTR of BMV RNA3 is not required for the formation of the RNA-dependent RNA polymerase complex (Quadt et al., 1995) or for replicase binding (Choi et al., 2004). Our results also show that the base-paired structure of BMV RNA3 exerts only modest effects on RNA amplification directed by BMV replicase compared with that directed by MYFV replicase (Fig. 6E). In the bromovirus CCMV, deletions of the regions containing the base-paired structure that corresponded to that of MYFV (Fig. 6A) had little effect on RNA3 accumulation, whereas deletions of another region of the 5′ UTR suppressed the accumulation of RNA3 and RNA4 (Pacha et al., 1990). Thus, although the 5′ UTR of bromovirus RNA3s might have general effects on the amplification of the negative-strand RNA3s of bromoviruses, it is not known whether the base-paired structures of BMV and CCMV RNA3s play roles during RNA3 replication by their own replicases. However, the base-paired structure of BMV was shown to function during the efficient amplification of RNA3 (Fig. 6), possibly by enhancing the amplification of negative-strand RNA3 in the presence of the heterologous replicase of MYFV. This variable requirement for the base-paired structure by distinct bromoviral replicases (Fig. 6E) suggests that in contrast to BMV, the base-paired structure in the 5′ UTR of RNA3 may be required for replicase assembly in MYFV.

In positive-strand RNA viruses, the transition from the translation to the replication of genomic RNAs is a key step during the RNA replication cycle because template competition

occurs between these two processes (Gamarnik and Andino, 1998). The *cis*-acting elements required for negative-strand synthesis have been found in the 5′ UTR of their genomic RNAs, and they are thought to regulate the transition through RNA–RNA interactions or RNA–protein interactions (Filomatori et al., 2006; Herold and Andino, 2001). In BMV, the repression of RNA1 and RNA2 translation is regulated by the interaction between the replicase protein 1a and the box B motif in their 5′ UTR, which may be related to replicase assembly (Chen et al., 2001; Yi et al., 2007), whereas the RNA3s of four bromoviruses including BMV and MYFV contain the box B motif in the intercistronic region. In two other bromoviruses, CCMV and broad bean mottle virus, the RNA3s do not even contain the box B motif (Allison et al., 1989; Romero et al., 1992). Thus, although some host factors have been reported to be involved in the translation and recruitment of BMV RNA3 (Diez et al., 2000; Mas et al., 2006), the detailed mechanisms that regulate translational repression and the transition from translation to replication in RNA3 are still unclear. In the present study, we identified a novel RNA element of MYFV RNA3, which is required for the efficient amplification of negative-strand in the 5′ UTR of RNA3, and we found that its function is MYFV replicase specific. These findings will facilitate the development of a better understanding of the life cycle of bromovirus RNA3.

Acknowledgments

This work was supported in part by a Grant-in-Aid for Scientific Research on Innovative Areas (24120006) from the Japanese Ministry of Education, Culture, Sports, Science and Technology, and a Grant-in-Aid for Scientific Research (B) (22380030) and a Grant-in-Aid for Scientific Research (A) (22248002) from the Japan Society for the Promotion of Science (JSPS). T.N. was a JSPS research fellow.

References

Allison, R.F., Janda, M., Ahlquist, P., 1989. Sequence of cowpea chlorotic mottle virus RNAs 2 and 3 and evidence of a recombination event during bromovirus evolution. Virology 172, 321–330.

Chen, J., Noueiry, A., Ahlquist, P. 2001. Brome mosaic virus protein 1a recruits viral RNA2 to RNA replication through a 5′ proximal RNA2 signal. J. Virol. 75, 3207–19.

Choi, S.K., Hema, M., Gopinath, K., Santos, J., Kao, C., 2004. Replicase-binding sites on plus- and minus-strand brome mosaic virus RNAs and their roles in RNA replication in plant cells. J. Virol. 78, 13420–13429.

Diez, J., Ishikawa, M., Kaido, M., Ahlquist, P., 2000. Identification and characterization of a host protein required for efficient template selection in viral RNA replication. Proc. Natl. Acad. Sci. U.S.A. 97, 3913–3918.

Dreher, T.W., 1999. Functions of the 3′-untranslated regions of positive strand RNA viral genomes. Annu. Rev. Phytopathol. 37, 151–174.

Filomatori, C.V., Lodeiro, M.F., Alvarez, D.E., Samsa, M.M., Pietrasanta, L., Gamarnik, A.V., 2006. A 5′ RNA element promotes dengue virus RNA synthesis on a circular genome. Gen. Dev. 20, 2238–2249.

French, R., Ahlquist, P., 1987. Intercistronic as well as terminal sequences are required for efficient amplification of brome mosaic virus RNA3. J. Virol. 61, 1457–1465.

Gamarnik, A.V., and Andino, R., 1998. Switch from translation to RNA replication in a positive-stranded RNA virus. Genes Dev. 12, 2293–2304.

Grdzelishvili, V.Z., Garcia-Ruiz, H., Watanabe, T., Ahlquist, P., 2005. Mutual interference between genomic RNA replication and subgenomic mRNA transcription in brome

mosaic virus. J. Virol. 79, 1438–1451.

Hema, M., Kao, C.C., 2004. Template sequence near the initiation nucleotide can modulate brome mosaic virus RNA accumulation in plant protoplasts. J. Virol. 78, 1169–1180.

Herold, J., Andino, R., 2001. Poliovirus RNA replication requires genome circularization through a protein-protein bridge. Mol. Cell 7, 581–591.

Higuchi, R., 1990. Recombinant PCR. in: Innis, M.A., Gelfand, D.H., Sninsky, J.J., and White, T.J. (Eds.), PCR Protocols. Academic Press, San Diego, pp. 177–183.

Iwakawa, H-O., Kaido, M., Mise, K., Okuno, T., 2007. *cis*-Acting core RNA elements required for negative-strand RNA synthesis and cap-independent translation are separated in the 3′-untranslated region of *Red clover necrotic mosaic virus* RNA1. Virology 369, 168–181.

Janda, M., French, R., Ahlquist, P., 1987. High efficiency T7 polymerase synthesis of infectious RNA from cloned brome mosaic virus cDNA and effects of 5′ extentions on transcript infectivity. Virology 158, 259–262.

Janda, M., Ahlquist, P., 1993. RNA-dependent replication, transcription, and persistence of brome mosaic virus RNA replicons in *S. cerevisiae*. Cell 72, 961–970.

Kaido, M., Mori, M.,Mise, K., Okuno, T., Furusawa, I., 1995. Inhibition of brome mosaic virus (BMV) amplification in protoplasts from transgenic tobacco plants expressing replicable BMV RNAs. J. Gen. Virol. 76, 2827–2833.

Kim, C.H., Kao, C.C., Tinoco, I.Jr. 2000. RNA motifs that determine specificity between a viral replicase and its promoter. Nat. Struct. Biol. 7, 415–423.

Komoda, K., Naito, S., Ishikawa, M., 2004. Replication of plant RNA virus genomes in a cell-free extract of evacuolated plant protoplasts. Proc. Natl. Acad. Sci. U.S.A. 101, 1863–1867.

Kovalev, N., Pogany, J., Nagy, P.D., 2014. A template role of double-stranded RNA in

tombusvirus replication. J. Virol. 88, (in press). doi:10.1128/JVI.03842-13.

Kroner, P., Ahlquist, P., 1992. RNA-based viruses. in: Gurr S.J., McPherson M.J., Bowles D.J. (Eds.), Molecular Plant Pathology; a Practical Approach, Vol 1. Oxford University Press, New York, pp. 23–34.

Kroner, P.A., Young, B.M., Ahlquist, P., 1990. Analysis of the role of brome mosaic virus 1a protein domains in RNA replication, using linker insertion mutagenesis. J. Virol. 64, 6110–6120.

Kroner, P., Richards, D., Traynor, P., Ahlquist, P., 1989. Defined mutations in a small region of the brome mosaic virus 2 gene cause diverse temperature-sensitive RNA replication phenotypes. J. Virol. 63, 5302–5309.

Liu Y, Wimmer E, Paul AV. 2009. Cis-acting RNA elements in human and animal plus-strand RNA viruses. Biochim. Biophys. Acta. 1789, 495–517.

Mas, A., Alves-Rodrigues, I., Noueiry, A., Ahlquist, P., Diez, J. 2006. Host deadenylation-dependent mRNA decapping factors are required for a key step in brome mosaic virus RNA replication. J. Virol. 80, 246–251.

Miller, W.A., Dreher, T.W., Hall, T.C. 1985. Synthesis of brome mosaic virus subgenomic RNA in vitro by internal initiation on (-)-sense genomic RNA. Nature 313, 68–70.

Mine, A., Takeda, A., Taniguchi, T., Taniguchi, H., Kaido, M., Mise, K., Okuno, T., 2010. Identification and characterization of the 480-kilodalton template-specific RNA dependent RNA polymerase complex of *Red clover necrotic mosaic virus*. J. Virol. 84, 6070–6081.

Mise, K., Allison, R.F., Janda, M., and Ahlquist, P., 1993. Bromovirus movement protein genes play a crucial role in host specificity. J. Virol. 67, 2815–2823.

Narabayashi, T., Iwahashi, F., Kaido, M., Okuno, T., Mise, K., 2009. *Melandrium yellow fleck bromovirus* infects *Arabidopsis thaliana* and has genomic RNA sequence

characteristics that are unique among bromoviruses. Arch. Virol. 154, 1381–1389.

Noueiry, A.O., Ahlquist, P., 2003. Brome mosaic virus RNA replication: revealing the role of the host in RNA virus replication. Annu. Rev. Phytopathol. 41, 77–98.

Ogram, S.A., Flanegan, J.B., 2011. Non-template functions of viral RNA in picornavirus replication. Curr. Opin. Virol. 1, 339–346.

Pacha, R.F., Allison, R.F., Ahlquist, P., 1990. *cis*-Acting sequences required for in vivo amplification of genomic RNA3 are organized differently in related bromoviruses. Virology 174, 436–443.

Pathak, K.B., Pogany, J., Nagy, P.D., 2011. Non-template functions of the viral RNA in plant RNA virus replication. Curr. Opin. Virol. 1, 332–338.

Quadt, R., Ishikawa, M., Janda, M., Ahlquist, P., 1995. Formation of brome mosaic virus RNA-dependent RNA polymerase in yeast requires coexpression of viral proteins and viral RNA. Proc. Natl. Acad. Sci. U.S.A. 92, 4892–4896.

Romero, J., Dzianott, A.M., Bujarski, J.J., 1992. The nucleotide sequence and genome organization of the RNA2 and RNA3 segments in broad bean mottle virus. Virology 187, 671–681.

Sarawaneeyaruk, S., Iwakawa, H.O., Mizumoto, H., Murakami, H., Kaido, M., Mise, K., Okuno, T., 2009. Host-dependent roles of the viral 5′ untranslated region (UTR) in RNA stabilization and cap-independent translational enhancement mediated by the 3′ UTR of *Red clover necrotic mosaic virus* RNA1. Virology 391, 107–118.

Schwartz, M., Chen, J., Janda, M., Sullivan, M., den Boon, J., Ahlquist, P., 2002. A positive-strand RNA virus replication complex parallels form and function of retrovirus capsids. Mol. Cell 9, 505–514.

Sullivan, M.L., Ahlquist, P., 1999. A brome mosaic virus intergenic RNA3 replication signal functions with viral replication protein 1a to dramatically stabilize RNA in vivo. J. Virol.

73, 2622–2632.

Yi, G., Gopinath, K., Kao, C.C., 2007. Selective repression of translation by the brome mosaic virus 1a RNA replication protein. J. Virol. 81, 1601–1609.

Zuker, M., 2003. Mfold web server for nucleic acid folding and hybridization prediction. Nucleic Acids Res. 31, 3406–3415.

Figure captions

Fig. 1. Competition between 3W and 3S in *Nicotiana benthamiana* protoplasts. (A) Schematic representation of the 5′ UTR of 3W and 3S. The open bar indicates the 5′ terminal region that is not duplicated. The light-gray region represents the duplicate region of the dark-gray region in the 5′ UTR of melandrium yellow fleck virus (MYFV) RNA3. Schematic representations of the predicted structures are also shown. Supplementary Fig. S1 shows the predicted structures based on nucleotide sequences. (B) Northern blot analysis of viral RNA accumulation in *N. benthamiana* protoplasts inoculated with a mixture of equimolar amounts of 3W and 3S, and MYFV RNA1 and RNA2. Ethidium bromide-stained rRNA is shown as a loading control. (C) The histogram represents the accumulation ratios of 3W compared with 3S during competition. The levels were measured using the ImageJ program, and the mean value and the standard deviation were calculated based on six independent experiments.

Fig. 2. Deletion analysis of the 5′ UTR of melandrium yellow fleck virus (MYFV) RNA3. (A) Schematic representation of the deleted regions in the 5′ UTR of 3S. Nucleotide deletions are indicated by bent lines where the nucleotide numbers are shown at their 5′ and 3′ ends. (B) Northern blot analysis of viral RNA accumulation in *Nicotiana benthamiana* protoplasts inoculated with 3S or its variants, together with MYFV RNA1 and RNA2.

Fig. 3. Structure-based deletion analysis of the 5′ UTR of melandrium yellow fleck virus (MYFV) RNA3. (A) Schematic representations of the predicted secondary structures of the regions, including the *cis*-element involved in 3S amplification. (B) Schematic representations of the deleted regions in the 5′ UTR of 3S. Nucleotide deletions are indicated by bent lines where the nucleotide numbers are shown at their 5′ and 3′ ends. (C) Northern

blot analysis of viral RNA accumulation in *Nicotiana benthamiana* protoplasts inoculated with 3S or its variants, together with MYFV RNA1 and RNA2.

Fig. 4. Analysis of the *cis*-acting RNA elements required for the efficient amplification of melandrium yellow fleck virus (MYFV) RNA in vivo. (A) Schematic representation of the secondary structure of the base-paired region. The disrupted and restored helical regions are shown. Substituted nucleotides are indicated by boldface italic fonts. (B) Northern blot analysis of positive (+)- and negative (–)-strand RNA accumulation in *Nicotiana benthamiana* protoplasts inoculated with 3S or its variants, together with MYFV RNA1 and RNA2. (C) Relative accumulation of positive- or negative-strand RNA3 by upper stem mutants compared with that using 3S. The histogram compares the levels of the positive strand (dark-gray bars) or negative strand (light-gray bars) of the tested RNA3 derivatives with that of the positive or negative strand of 3S, respectively. The levels were measured using the ImageJ program, and the mean value and the standard deviation were calculated based on three independent experiments.

Fig. 5. In vitro RNA replication assay of the upper stem mutants of melandrium yellow fleck virus (MYFV) RNA3. (A) Accumulation of positive- and negative-strand RNA3 in evacuolated BY-2 protoplast lysates incubated for 2 h with mRNA that expressed MYFV 1a and 2a proteins, followed by 2 h with 3S or its variants. The total RNA was extracted and subjected to Northern blot analysis. (B) The activity of negative-strand RNA3 synthesis shown by the relative RNA3(-)/RNA3(+) ratio of the tested RNA3 derivatives compared with that of 3S. The levels were measured using the ImageJ program, and the mean value and the standard deviation were calculated based on three independent experiments.

Fig. 6. Functional analysis of the similar base-paired structure of brome mosaic virus (BMV) RNA3. (A) Predicted secondary RNA structures in the 5′ UTR of RNA3 for six bromoviruses, including base-paired regions (surrounded by dotted lines). The secondary RNA structures were predicted using M-fold (Zuker, 2003). Accession numbers of the nucleotide sequences of bromovirus RNA3s and ΔG (kcal/mole) values of the predicted structures of the 5′ UTRs: melandrium yellow fleck virus (MYFV, NC_013268; ΔG = -46.8), BMV (NC_002028; ΔG = -20.3), cowpea chlorotic mottle virus (CCMV, NC_003542; ΔG = -56.6), cassia yellow blotch virus (CYBV, NC_007001; ΔG = -31.8), spring beauty latent virus (SBLV, NC_004122; ΔG = -49.9), and broad bean mottle virus (BBMV, NC_004006; ΔG = -69.3). (B) Schematic images of the base-paired regions of 3S and its derivatives. The deleted regions and a four-nucleotide insertion are indicated by dotted lines and boldface italic letters, respectively. (C) Northern blot analysis of viral RNA accumulation in *Nicotiana benthamiana* protoplasts inoculated with 3S or its variants, together with MYFV RNA1 and RNA2 (MY1+MY2). The numbers below the panel represent the accumulation levels of RNA3 relative to the internal standard (coinoculated RNA1 and RNA2) and those of RNA4 relative to RNA3. The levels were measured using the ImageJ program, and the mean values were calculated based on three independent experiments. (D) Schematic images of the corresponding structures of BMV RNA3 and its derivatives. The dotted lines indicate deleted regions. (E) Northern blot analysis of viral RNA accumulation in *N. benthamiana* protoplasts inoculated with BMV RNA3 or its variants, together with RNA1 and RNA2 of BMV (B1+B2) or the corresponding MYFV RNAs (MY1+MY2). The levels were measured using the ImageJ program, and the mean values were calculated based on three independent experiments.

Supplementary Fig. S1. Predicted structures of the 5′ UTR of 3W and 3S. The secondary RNA structures were predicted using M-fold (Zuker, 2003).

Supplementary Fig. S2. Temporal changes in the accumulation patterns of 3S and its derivatives in two independent experiments (#1 and #2). RNAs were incubated in a cell-free extract of evacuolated BY-2 protoplasts (BYL). Total RNAs extracted from BYL at the indicated times after incubation were subjected to Northern blot analysis using DIG-labeled RNA probe specific to the 3′UTR of RNA3. Relative values for the accumulation of RNAs were calculated and are shown between a pattern on a Northern blot and ethidium-bromide-stained rRNA.

Supplementary Table S1

List of PCR primers and the nucleotide sequences used to generate constructs

Primer name	Sequence
M4	GTTTTCCCAGTCACGAC
MY3.13R-2	GGTGCACTCTTGATTATC
d55-153_F	CAACTAATTGGACGGCTTGGAAGAAAATAC
d55-153_R	CCAAGCCGTCCAATTAGTTGCTTTATCGG
d104-202_F	CGGTGTATCTCCGAAACTTTAGATTG
d104-202_R	CTAAAGTTTCGGAGATACACCGAAACG
d154-226_F	GTCCTCCCGTTAAAATGTCTAACCTAGTTAAAC
d154-226_R	TTAGACATTTTAACGGGAGGACCTACTAAC
d154-252_F2	GGTCCTCCCGTTATGACAGGTCGTTCTTC
d154-252_R2	CGACCTGTCATAACGGGAGGACCTACTAAC
d55-64_F	AAAGCAACTAATTCTTTTTCTTTTTTTTCC
d55-64_R	AAAAGAAAAAGAATTAGTTGCTTTATCGG
d65-81_F	TTGTAGAATTTAAATTTATCGTTTCGGTG
d65-81_R	CGATAAATTTAAATTCTACAATTAGTTGC
d82-103_F	CTTTTTTTTCCTTAAGGTTGGAACACACAG
d82-103_R	GTTCCAACCTTAAGGAAAAAAAAAGAAAAAG
d203-217_F	CCTCTCAGCGTTCGTTTTAAAGAAAATGTC
d203-217_R	CTTTAAAACGAACGCTGAGAGGAATTATAG
d218-229_F	AACTTTAGATTATGTCTAACCTAGTTAAAC
d218-229_R	CTAGGTTAGACATAATCTAAAGTTTCGGG
r1-1_F	GCGTTCGGCTTTGTTTAGATTGTTTTAAAG
r1-1_R	AACAAAGCCGAACGCTGAGAGGAATTATAG
r1-2_F	ATTTATCCAAAGCCTGTATCTTTAAGGTTG
r1-2_R	TACAGGCTTTGGATAAATTGGAAAAAAAAG
r2-1_F	CCGAAACTTATTTAAGTTTTAAAGAAAATG
r2-1_R	CTTTAAAACTTAAATAAGTTTCGGGAACGC
r2-2_F	TCCTTAGATTCGTTTCGGTGTATCTTTAAG
r2-2_R	GAAACGAATCTAAGGAAAAAAAAGAAAAAG
dMB-1_1	ATTGTAGAATTTACGGTGTATCTTTAAGG
dMB-1_2	TTAAAGATACACCGTAAATTCTACAATTAG
dMB-1_3	CAGCGTTCCCGATGTCTAACCTAGTTAAAC
dMB-1_4	TTAACTAGGTTAGACATCGGGAACGCTGAG
dMB-2_1	TGTAGAATTTAACATCGGTGTATCTTTAAG
dMB-2_2	TACACCGATGTTAAATTCTACAATTAGTTG
dMB3_F	AGTAGTGATACTGTTTTTGTTCCCGATGTCTAACCTAGTTAAAC
dMB3_R	CAAAAACAGTATCACTACTGAAAAAACCGATGTTAAATTCTAC
pBYL-MY1a_F	ATAAGAATGGCGCGCCATGGATCTATTAAATTTAATTG
pBYL-MY1a_R	ATAAGAATGGCGCGCCTCAACTTACGCAAGCATC
pBYL-MY2a_F	ATAAGAATGGCGCGCCATGGCTTTCGAAATTGAATATG
pBYL-MY2a_R	ATAAGAATGGCGCGCCTTACTTAGAAAAAGAAGAC
Bd1_F	TAGTGATACTATGTCTAACATAGTTTCTCC
Bd1_R	TTAGACATAGTATCACTACTGAAAAAACCG
Bd2_F	CTATTTTACCAATGTCTAACATAGTTTCTC
Bd2_R	GTTAGACATTGGTAAAATAGAATGTTCGCC

Fig. 1

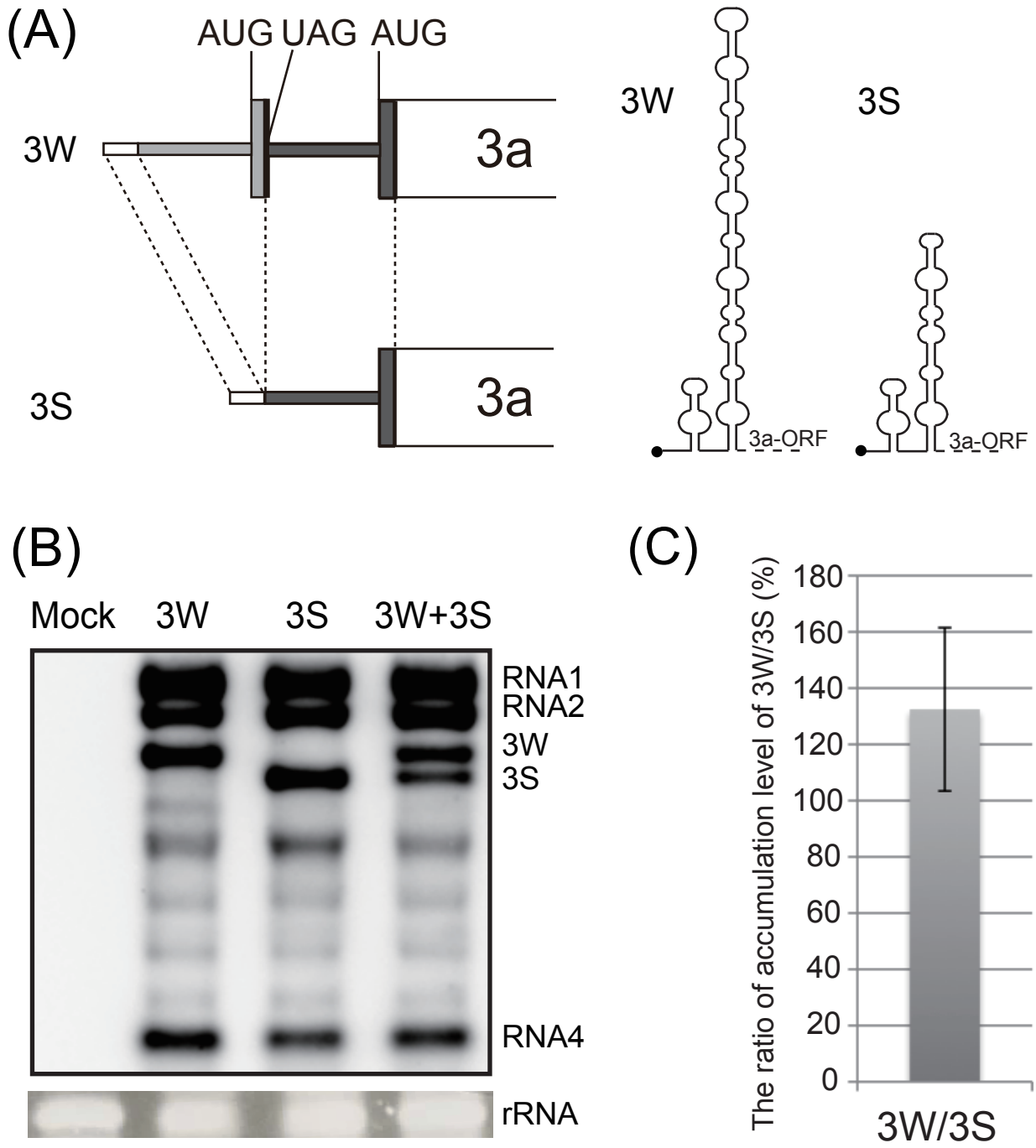

Fig. 2

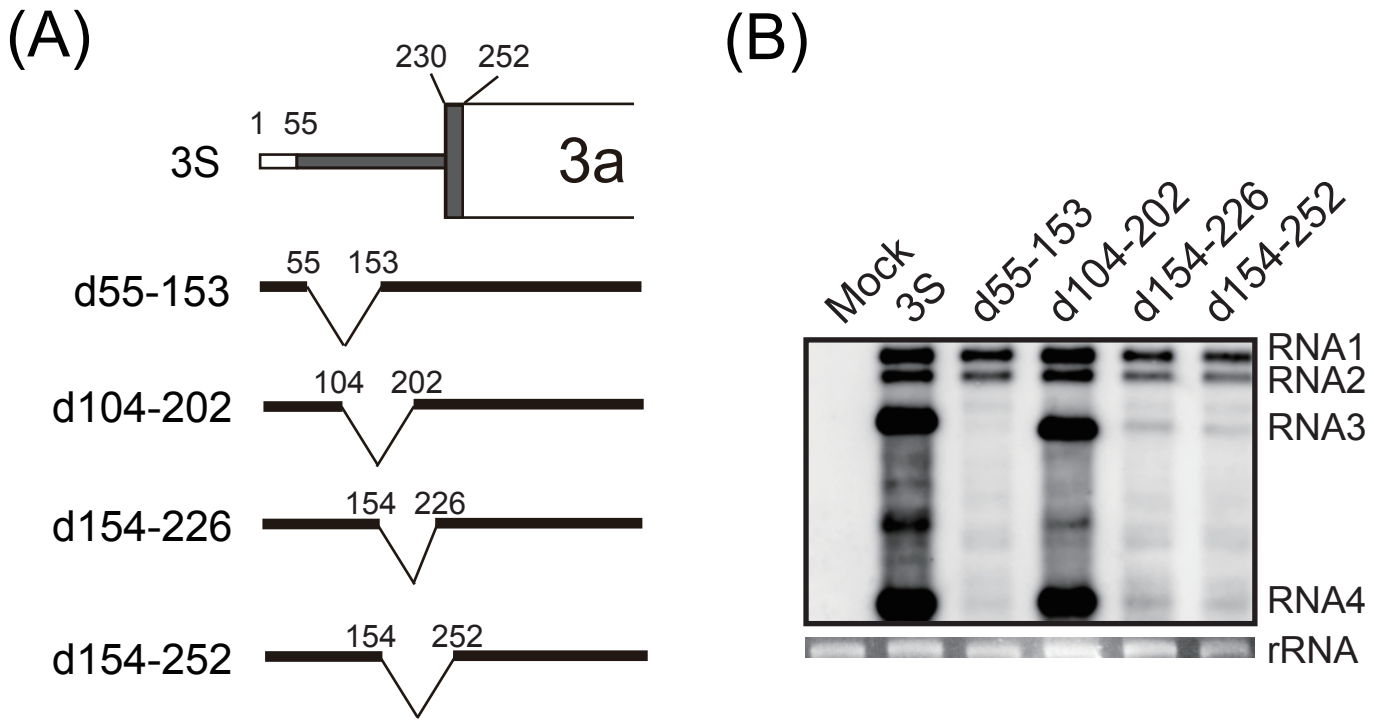

Fig. 3

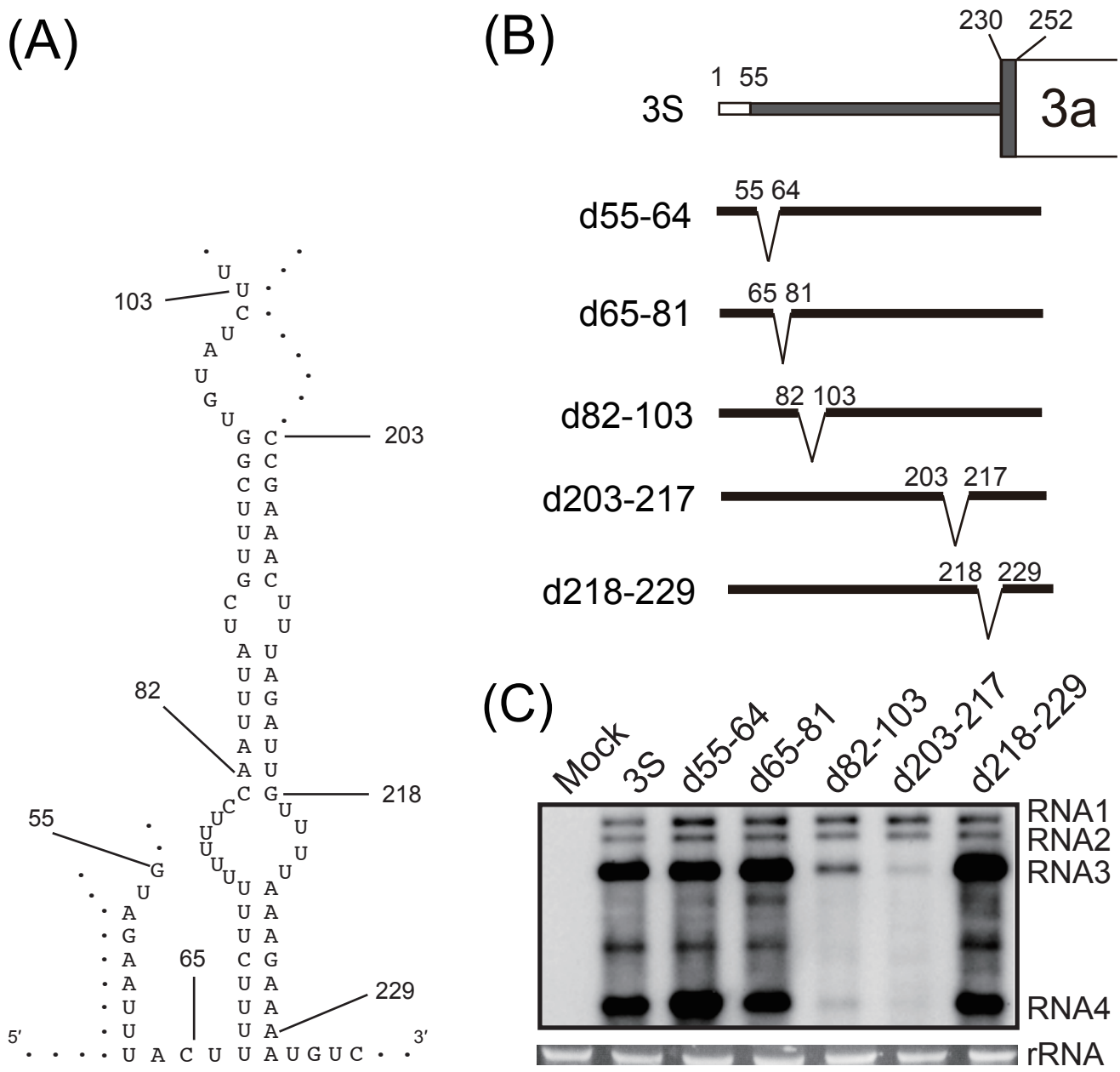

Fig. 4

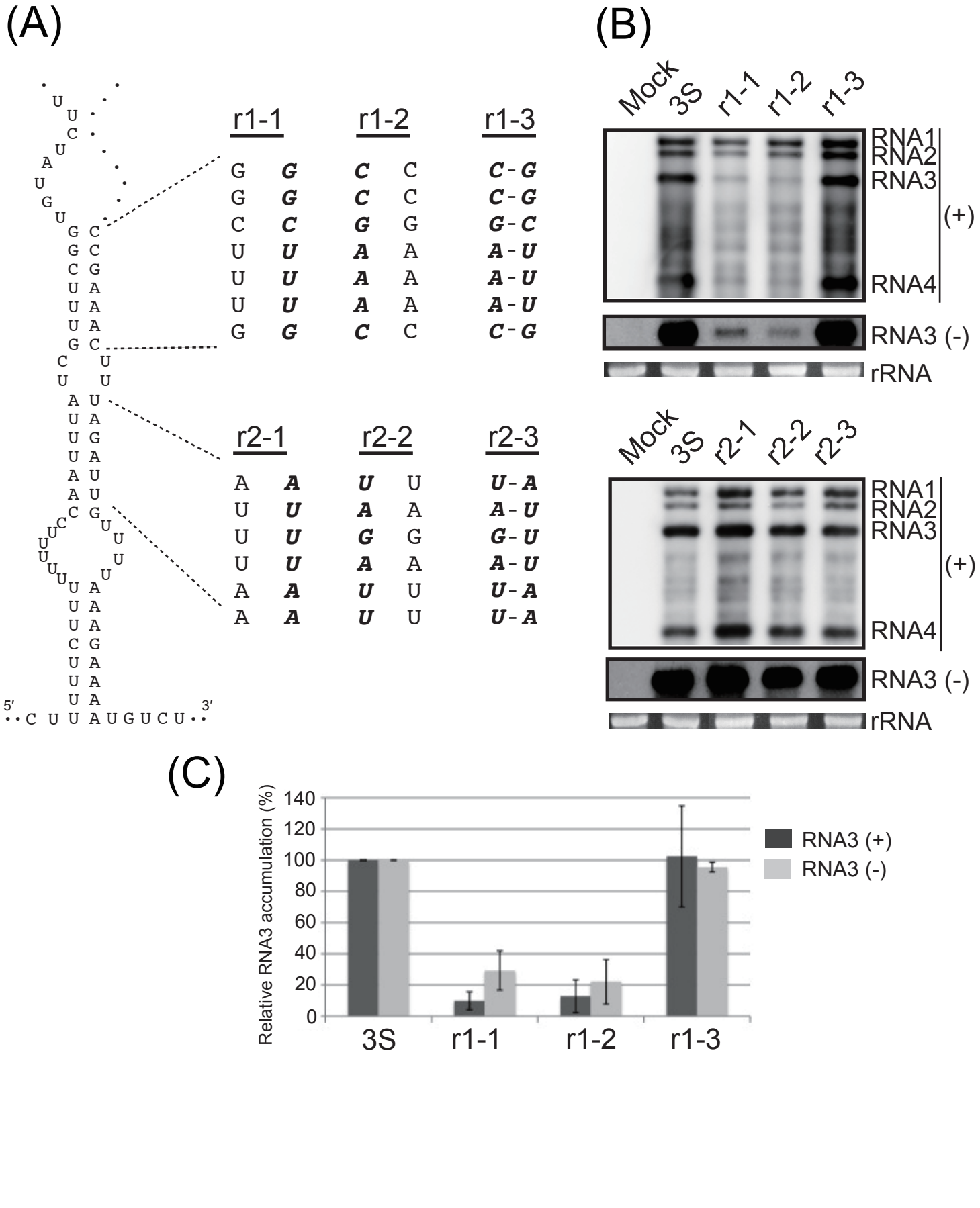

Fig. 5 (Revised)

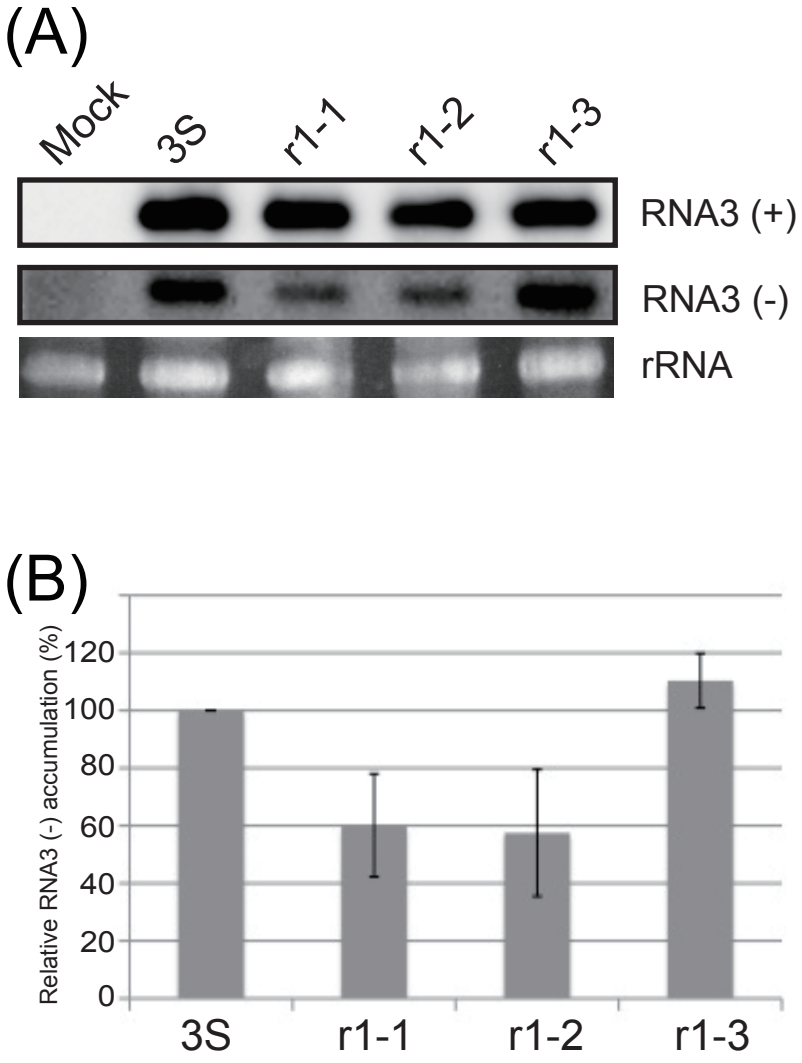

Fig. 6 (Revised)

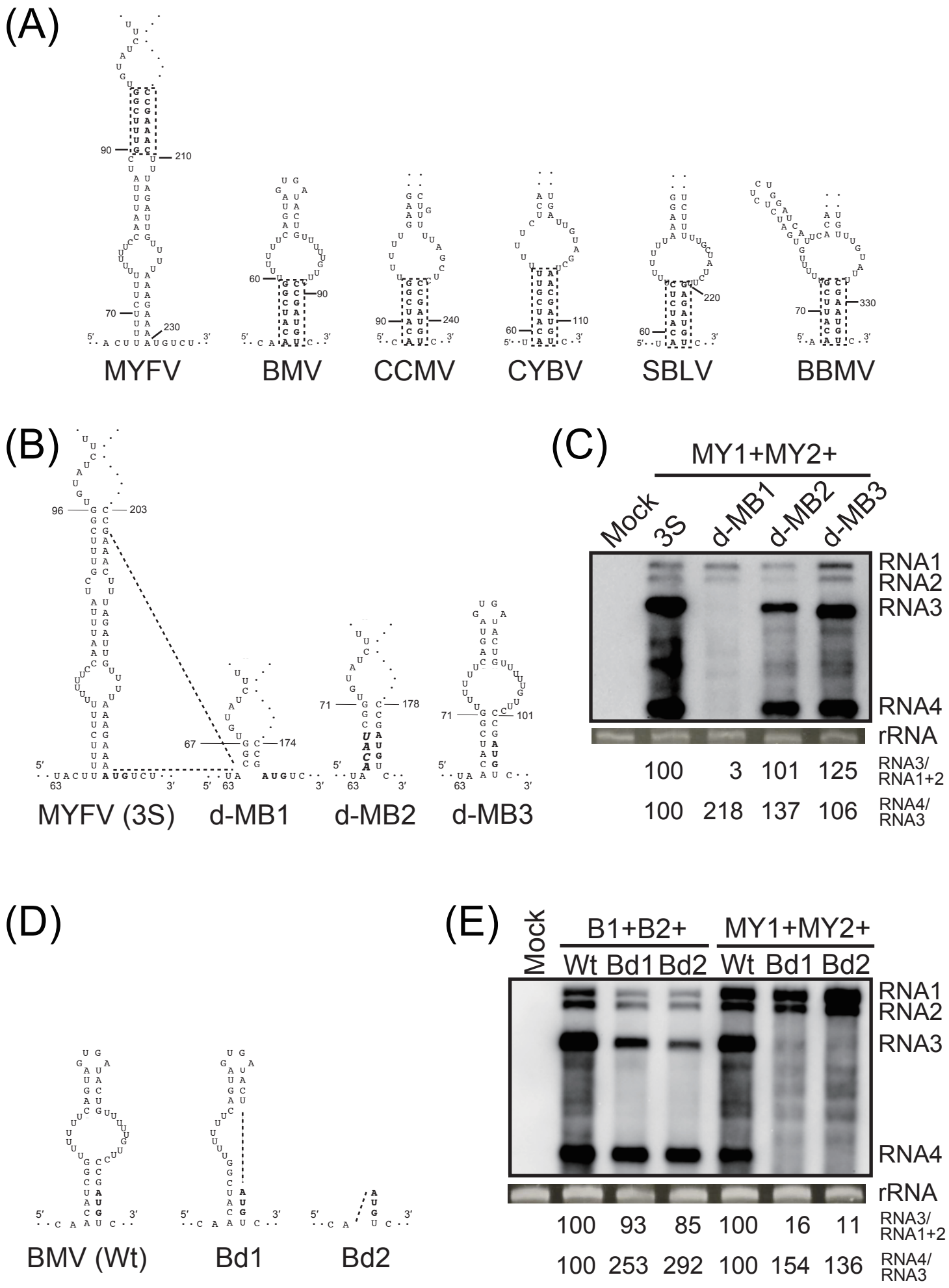

Supplementary Fig. S1

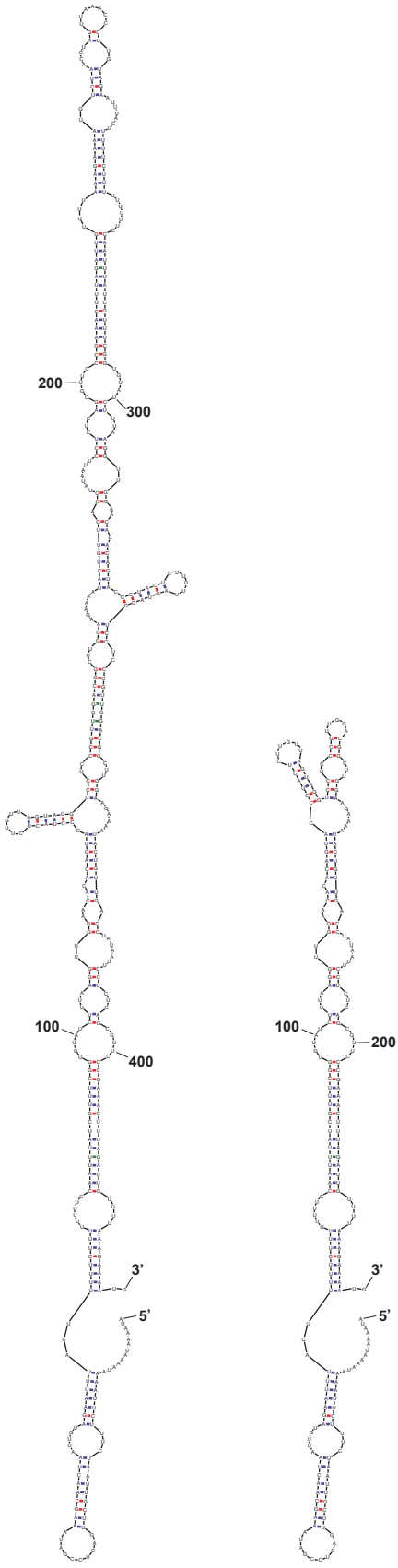

3W **3S**

Supplementary Fig. S2